

## **EXPERIMENTAL INVESTIGATION INTO THE FATIGUE CRACK GROWTH IN CONCRETE**

S. Cangiano,  
CTG-Italcementi Group, Bergamo, Italy  
G.A. Plizzari,  
University of Brescia, Department of Civil Engineering, Italy  
V. Slowik,  
Hochschule für Technik, Wirtschaft und Kultur Leipzig (FH), Germany

### **Abstract**

The aim of the present work is to contribute to a better understanding of the fatigue behavior of cracked concrete. Cyclic direct tension tests of cylindrical specimens made of normal strength concrete as well as high-strength concrete with and without steel and carbon fibers were performed. The material response obtained in the direct tension tests is compared to the structural response measured in bending tests.

Key words: Fatigue, Concrete, Cracking, Fracture Mechanics, Fibers

### **1 Introduction**

Although much research has been done on the fatigue behavior of concrete subjected to compression, the problem of crack propagation in concrete specimens subjected to cyclic loading is still open to further investigation. It is commonly accepted that the concrete damage under fatigue loading mainly occurs in the Fracture Process Zone (FPZ) present at the crack tip. Slowik, Plizzari and Saouma (1996) have shown that after applying comparatively high pre-peak loads to concrete wedge splitting specimens, during the following cyclic loading the crack

propagation rate remarkably increased. This rate increase was attributed to the presence of a larger FPZ after the application of some “spikes” in the loading history.

The presence of fatigue damage in the FPZ of a concrete structure would explain the sequence effect found by some researchers who tested “structural specimens” such as beams or wedge splitting specimens (Oh, 1991; Hordijk, 1991). In these specimens the FPZ size strongly depends on the loading history as well as on the specimen size (Bazant and Shell, 1993). This would also explain the inapplicability of the Palmgren-Miner rule (Miner, 1945) to determine the fatigue strength of concrete structures (Hilsdorf and Kesler, 1964).

The fatigue behavior of concrete structures can be correctly studied only when the material behavior in the FPZ is known; it can be determined by performing cyclic direct tension tests on cracked specimens. Experimental results available in the literature have evidenced that the ultimate displacements of specimens subjected to cyclic loading are very close to the load-displacement curve (envelope curve) obtained in corresponding static tests (Hordijk, 1991; Plizzari et al., 1997a). This aspect may be particularly meaningful for fiber-reinforced concrete characterized by high post-cracking stresses and deformations. The use of fibers can prove to be even more effective in high-strength concrete which, on account of the intragranular nature of the cracking phenomenon, is characterized by a comparatively brittle fracture behavior.

Since loading reversals may occur at any moment during the loading history, the material should be studied both for the cycles on the envelope curve and the inner loops (Fig. 1b). Experimental results for cycles that follow the critical softening envelope curve have been presented by Gylltoft (1983), Reinhardt et al. (1986), and Hordijk (1991), whereas tests with inner loops were performed by Plizzari et al. (1997a).

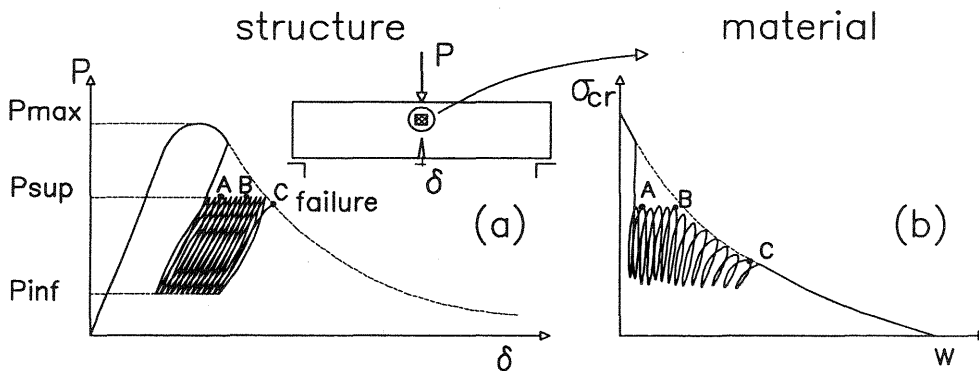


Fig. 1. Structure (a) and material (b) response

The aim of the present work is to shed some new light on fatigue behavior of high-performance concrete by performing direct tension tests. For comparison, normal strength concrete as well as high-strength concrete have been included and tests were conducted on notched as well as on unnotched cylindrical specimens. Furthermore, the effect of steel and carbon fibers was a subject of this investigation.

The results obtained allow to make a preliminary comparison between the different types of concrete and between the material and structural behavior. The latter can be done by contrasting the present results with those obtained from four-point bending beams made of the same concrete (Plizzari et al., 1997b).

## 2 Experiments

### 2.1 Direct tension tests on notched specimens

The cylinders had a diameter of 80 mm and a height of 210 mm. They were demoulded 24 hours after casting; the subsequent curing was performed under water at  $20 \pm 2^\circ\text{C}$  for at least 60 days. A triangularly shaped notch, 4 mm deep, was cut into the middle section of the specimen reducing the diameter to 72 mm (Fig. 2).

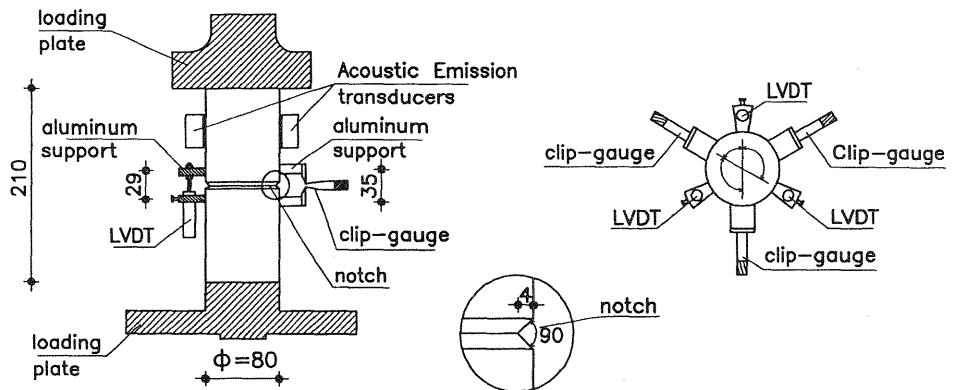


Fig. 2. Experimental setup for testing the notched specimens

The concrete samples contained siliceous aggregates having a rounded shape and a maximum diameter of 15 mm. The grain size distribution was very close to the Bolomey curve. Two types of cement, class 32.5 R type CEM II/B-L (UNI-ENV 197) for normal strength concrete, and class 52.5 R type CEM I (UNI-ENV 197) for high-strength concrete were used. Silica fume "Elkem microsilica grade 940-U" was also used in high-strength concrete.

Two different types of fibers have been added to the concrete: hooked steel fibers type “Dramix ZP 30/0.50” ( $l=30\text{mm}$ ,  $\phi=0.5\text{mm}$ ), and polyacrylonitrile (carbon) fibers type “RK10” ( $l=20\text{mm}$ ,  $\phi=0.008\text{mm}$ ).

With the materials described above, normal-strength (NSC) and high-strength concretes (HSC) have been prepared. For both concretes, mixes with and without fibers were produced. The usage of carbon fibers was limited to HSC only. The NSC and HSC concretes reinforced with steel fibers will be identified as NSC-SFR and HSC-SFR, respectively, while those reinforced with carbon fibers are referred to as HSC-CFR. A low volume fraction of fibers was chosen ( $V_f=0.38\%$ ) for both steel and carbon fibers.

Table 1 shows the concrete mix proportions and some material properties. The compressive strength ( $f_c$ ), the uniaxial tensile strength ( $f_{ct}$ ), and the elastic modulus of elasticity ( $E_c$ ) were measured from cylinders after 28 days of curing in water at  $20^\circ\text{C}$ .

Table 1. Mix-design, fresh-state properties and mechanical properties of the adopted concretes

Type of Concrete	Cement [kg/m <sup>3</sup> ]	Silica fume [kg/m <sup>3</sup> ]	w/c ratio	Slump [mm]	$F_c$ [MPa]	$f_{ct}$ [MPa]	$E_c$ [MPa]
NSC	370	-	0.56	130	45.4	4.01	31629
NSC-SFR	370	-	0.59	130	27.8	4.31	27368
HSC	550	55	0.29	200	102.0	5.16	48891
HSC-SFR	550	55	0.29	170	106.4	5.57	49383
HSC-CFR	550	55	0.29	100	96.5	5.18	49978

In the direct tension tests, the crack-opening data was acquired by three LVDTs (Linear Variable Differential Transformers) placed diametrically with a base length of 29 mm (Fig. 2). In addition, three resistance full-bridge displacement transducers (clip-gages) were fixed between the three LVDTs. The output from the three clip-gages was averaged by coupling them in parallel; the resulting signal was used as the feed-back signal.

A rigid coupling of the specimens to the loading system was obtained by two loading plates (Fig. 2). The specimens were glued to the plates, previously bolted to the loading system, by an epoxy resin.

During the tests the Acoustic Emission (A.E.) was monitored by means of two pre-amplifying transducers (range 0-50 MHz) attached to opposite sides of the specimen (Fig. 2). Silicone grease served as a coupling medium. The A.E. activity was acquired in terms of a cumulative count of acoustic events which is considered a measure for the development of the cracking process during the test.

The procedure of the cyclic tests can be subdivided into four stages, see Fig. 3. For the control a special software has been developed (Plizzari et al., 1997a).

- In the first stage (**OAB**), a constant rate for the COD was imposed up to the peak load. When the softening branch of the load-displacement curve began, and the load dropped to  $\approx 95\%$  of the peak load, the reference signal was inverted and the load decreased up to the lower limit  $P_{inf}$  of the following cyclic stage (point B, Fig. 3).
- In the second stage (**BC**), the COD is cycled at a frequency of about 1Hz; the inversion of the reference signal takes place whenever the upper and lower limits ( $P_{sup}$  and  $P_{inf}$ ) are reached; these limit values are input data expressed as a percentage of the peak load and were here equal to 25% and 75% of  $P_{max}$ , respectively.
- In the third stage (**CD**), the software detects the interception of the envelope curve (**ACDE**). The test remains stable, however, because of the COD control. The cyclic loading continues also in this stage by inverting the reference signal (COD) whenever the load, after reaching the envelope curve, drops to  $\approx 95\%$  of the maximum load measured in the cycle (Fig. 3). This stage ends when the maximum load, detected on the envelope curve, becomes lower than the value  $k1 \cdot P_{inf}$ . The limit  $k1$  ( $>1$ ) is set before starting the test.
- In the fourth stage (**DE**), a monotonic increase of the COD is imposed until the load drops to 1% of the maximum load ( $P_{max}$ ). At this point the test is stopped.

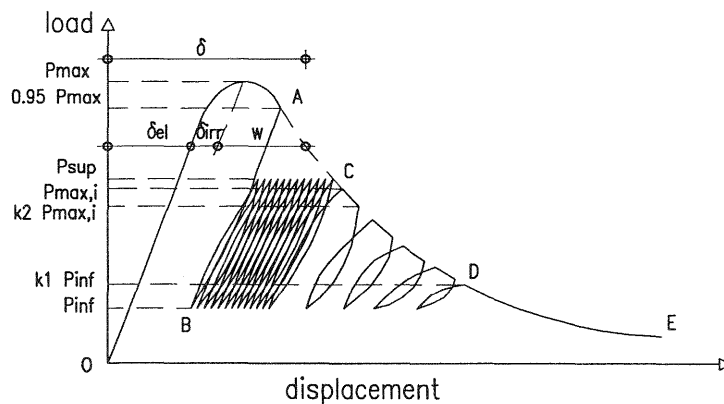


Fig. 3. Scheme of the loading history for cyclic tests under displacement control (Plizzari et al., 1997a)

## 2.2 Direct tension tests on unnotched specimens

For comparison, a number of cyclic direct tension tests was performed with unnotched specimens. Since there are no geometry induced stress

concentrations in such specimens, the development of the fracture process zone should depend on the characteristics of the tested material only. In order to prevent the specimens from failing at its end faces, a special set-up was designed (Wittmann et.al., 1994; Slowik, 1995). The cylindrical normal strength concrete specimen is glued between two high-strength concrete cylinders having the same cross section, see Fig. 4. The two concrete types do not differ significantly in their elastic properties. Therefore, the lateral restraint at the specimen end faces is minimized. Steel bars were loaded parallel to the specimen in order to increase the appearing stiffness of the loading system. The unnotched specimens had a diameter of 99 mm and a length of 50 mm.

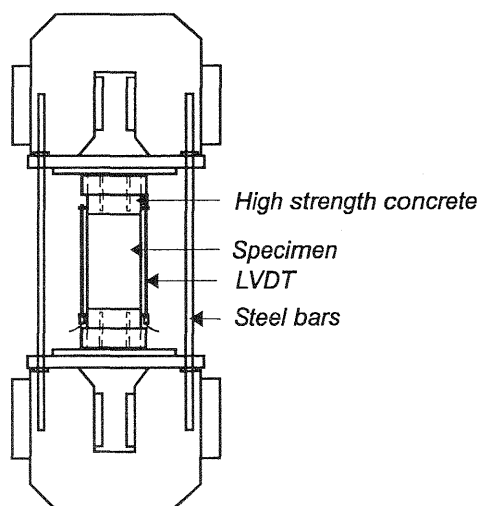


Fig. 4. Experimental setup for direct tension tests with unnotched specimens (Slowik, 1995)

The concrete used had a w/c ratio of 0.5 and a maximum aggregate size of 16 mm. All samples were drilled out of one block. At the age of testing (after about 200 days) the compressive strength amounted to 34 MPa and the uniaxial tensile strength to about 2.7 MPa.

The tests were started under displacement control. After the load had dropped to either 85%, 90%, 95%, or 98% of the peak load, the specimens were unloaded and, subsequently, subjected to a cyclic loading in the range of 25% to 75% of the maximum load. The cyclic loading was undertaken under load control with a frequency of 1 Hz. The tests became unstable when the displacement reached the envelope curve (point C in Fig. 3). By varying the level of unloading, the effect of the initial damage on the fatigue behavior was investigated.

### 3 Results and discussion

Fig. 5a exhibits a typical load-displacement curve as obtained from a notched high-strength concrete specimen with steel fibers. In the same figure, the cumulative number of A.E. events is plotted. It can be noted that the A.E. activity is very low during the inner loops and increases remarkably during the cycles on the envelope curve. This demonstrates that the fatigue damage mainly occurs during the cycles on the envelope curve. Figure 5b shows the Load-Crack Mouth Opening Displacement curve measured on a four point bending beam made of the same concrete (Plizzari et al., 1997b). Contrary to the direct tension test, the A.E. remarkably increases already during the inner loops. This evidences that, although the structure is subjected to inner loops, in some parts of the FPZ the material is subjected to cycles on the envelope curve and the concrete damage provokes A.E. events.

Fig. 6 exhibits load-displacement curves obtained in cyclic tests (points on the envelope curve) and in static tests on HSC-SFR and HSC-CFR specimens, respectively. The envelope curves match the static curves for both the materials quite well. This shows that the envelope curve for the fiber reinforced concrete can be approximated with the static monotonic curve, as already found for normal strength concrete without fibers by Hordijk (1991) and Plizzari et al. (1997a).

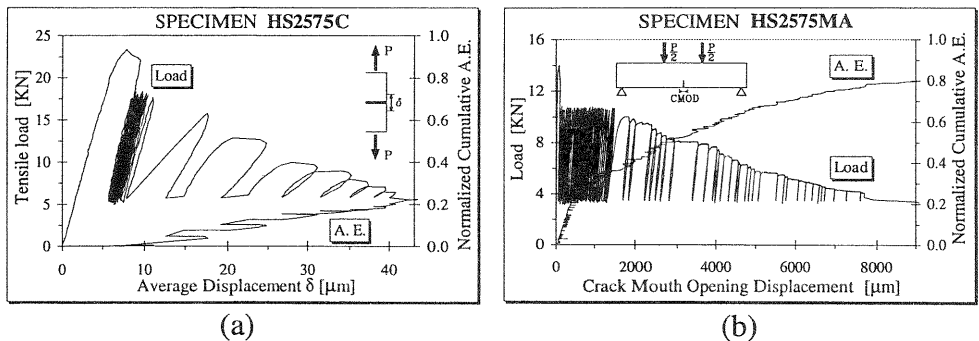


Fig. 5. Results of direct tension (a) and bending (b) tests, on high strength concrete specimens with steel fibers (In Fig. 5a not all load cycles are shown.)

Fig. 7 shows the influence of fibers in high-strength concrete on the post peak response. For the adopted volume fraction of fibers (0.38%), the carbon fibers did not significantly modify the load-displacement curve with respect to the plain concrete. The effect of steel fibers begins at a tensile stress of about 3.5 MPa in the post-peak region (corresponding here to a load of about 14 kN) and becomes significant at stresses lower than 1.7 MPa (corresponding here to a load of about 7 kN).

For higher cyclic load levels, the fibers play a minor role and no significant differences between plain and fiber reinforced concrete should be expected. However, for higher fiber contents the influence on the post-peak response is expected to be stronger.

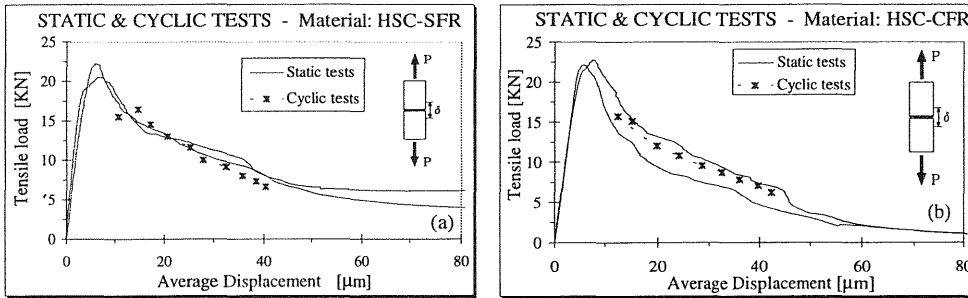


Fig. 6. Load-displacement curves from cyclic and static direct tension tests on NSC-SFR (a) and on HSC-CFR (b) specimens.

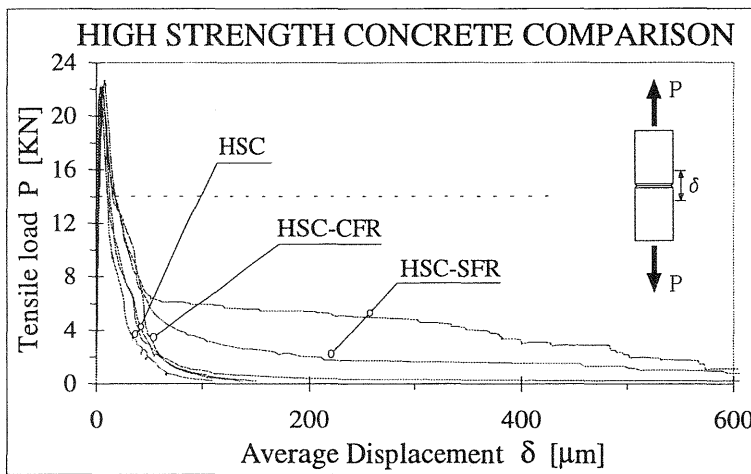


Fig. 7. Load-displacement curves as obtained in static direct tension tests on high-strength concrete cylinders.

Table 2 contains the maximum numbers of inner loops ( $N_{max}$ ) measured from notched cylinders subjected to a cyclic loading between 25% and 75% of the maximum load. The value of  $N_{max}$  is influenced by the addition of both types of fibers (steel or carbon). The effect of steel fibers is more pronounced in HSC than in NSC. Carbon fibers have less influence on  $N_{max}$  than steel fibers.

Table 2. Number of inner loops applied to notched cylindrical specimens

Material	NSC	NSC-SFR	HSC	HSC-SFR	HSC-CFR
$N_{max}$	344	1293	2	2685	1015

Characteristic results from the cyclic tests on the unnotched specimens are shown in Table 3. As mentioned above, after a certain percentage of the maximum load was reached in the post-peak region, a cyclic loading was imposed. The higher this percentage the higher the maximum cycle number. This is attributed to the different levels of microcracking and fracture process zone formation. The assumption that fatigue in concrete mainly occurs in the fracture process zone and not in the undamaged materials is supported by this observation.

Table 3. Number of inner loops applied to unnotched cylindrical specimens

	Unloading and start of the cyclic loading after			
	85%	90%	95%	98%
$N_{max}$	164	3352	3460	5114

The maximum numbers of load cycles measured on the unnotched specimens are significantly larger than those for the notched normal strength concrete specimens. A possible reason for this discrepancy might be the notches causing stress concentrations and supporting the development of the fracture process zone. However, it has to be taken into account that the scatter of experimental results from cyclic tests is usually large and that the experimental results were obtained for concretes having different mechanical properties. For a clarification more experiments should be performed.

#### 4 Conclusions

The main results can be summarized as follows:

- The envelope curves obtained from the cyclic tests match the curves obtained from the static tests on cylinders of fiber reinforced concrete quite well, as already found for normal concrete without fibers (Fig. 6).
- The comparison between the A.E. recorded in direct tension and bending tests, respectively, shows that in some parts of the FPZ of beams subjected to inner loops, the material is locally subjected to load cycles on the envelope curve (Fig.5).

- The number of inner loops  $N_{\max}$  obtained in direct tension tests is significantly influenced by the size of the FPZ and by the presence of fibers (Tab. 2). The effect of steel fibers is stronger in HSC than in NSC.

## 5 References

- Bazant, Z.P. and Shell W.F. (1993) Fatigue fracture of high-strength concrete and size effect. **ACI Materials Journal**, 90(5), 472-478.
- Gylltoft K. (1983) Fracture Mechanics Models for Fatigue in Concrete Structures. Doctoral Thesis, **Luleå University of Technology**.
- Hilsdorf H.K. and Kesler C.E. (1964) Fatigue strength of concrete under varying flexural stresses. **J. of the Amer. Conc. Inst.**, 63, 1059-1076.
- Hordijk D.A. (1991) Local approach to fatigue of concrete. Doctoral Thesis, **Delft University of Technology**.
- Miner M.A. (1945) Cumulative damage in fatigue. **J. of Applied Mechanics, Trans. ASME**, 12(1), A159-A164.
- Oh B.H. (1991) Cumulative damage theory of concrete under variable-amplitude fatigue loading. **ACI Materials Journal**, 88(1), 41-48.
- Plizzari G.A., Cangiano S. and Alleruzzo S. (1997a) The fatigue behavior of cracked concrete. **Fatigue & Fracture of Engineering Materials & Structures**, 20(8), 1195-1206.
- Plizzari G.A., Cangiano S. and Cere N. (1997b) Sul comportamento a frattura di travi fessurate in calcestruzzi ordinari, ad alta resistenza e fibrorinforzati. **Giornate AICAP 1997**, Rome, 1, 247-256, in Italian.
- Reinhardt H.W., Cornelissen H.A.W. and Hordijk D.A. (1986) Tensile Tests and Failure Analysis of Concrete. **ASCE Journal of Structural Eng.**, 112(11), 2462-2477.
- Slowik V. (1995) Beiträge zur experimentellen Bestimmung bruchmechanischer Materialparameter von Beton. Building Material Reports No. 3, AEDIFICATIO Publishers, Freiburg.
- Slowik V., Plizzari, G.A. and Saouma V. (1996) Fracture of concrete under variable amplitude loading. **ACI Materials Jour.**, 93, 272-283.
- Wittmann F.H., Slowik V. and Alvaredo A.M. (1994) Probabilistic aspects of fracture energy of concrete, **Materials and Structures**, 27, 499-504.